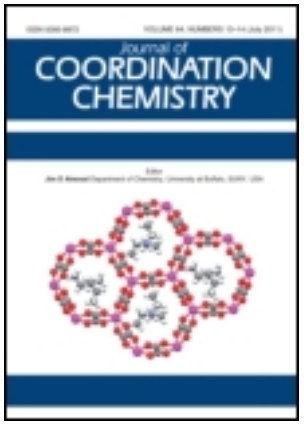

Journal of Coordination Chemistry
Publication details, including instructions for authors and subscription information:
http://www.tandfonline.com/loi/gcoo20

Metal complexes of porphyrin-anthraquinone hybrids: DNA binding and photocleavage specificities

Ping Zhao [a] , Jin-Wang Huang [b] & Liang-Nian Ji [b]

[a] School of Chemistry and Chemical Engineering, Guangdong Pharmaceutical University , No. 280, Waihuandong Road, Education Mega Centre, Guangzhou 510006 , P.R. China

[b] MOE Laboratory of Bioinorganic and Synthetic Chemistry , School of Chemistry and Chemical Engineering, Sun Yat-Sen University , No. 135, Xingangxi Road, Guangzhou 510275 , P.R. China

Published online: 25 May 2011.

To cite this article: Ping Zhao , Jin-Wang Huang & Liang-Nian Ji (2011) Metal complexes of porphyrin-anthraquinone hybrids: DNA binding and photocleavage specificities, Journal of Coordination Chemistry, 64:11, 1977-1990, DOI: 10.1080/00958972.2011.585641

To link to this article: http://dx.doi.org/10.1080/00958972.2011.585641

Journal of Coordination Chemistry
Vol. 64, No. 11, 10 June 2011, 1977–1990

Metal complexes of porphyrin–anthraquinone hybrids: DNA binding and photocleavage specificities

PING ZHAO*†, JIN-WANG HUANG‡ and LIANG-NIAN JI‡

†School of Chemistry and Chemical Engineering, Guangdong Pharmaceutical University, No. 280, Waihuandong Road, Education Mega Centre, Guangzhou 510006, P.R. China
‡MOE Laboratory of Bioinorganic and Synthetic Chemistry, School of Chemistry and Chemical Engineering, Sun Yat-Sen University, No. 135, Xingangxi Road, Guangzhou 510275, P.R. China

(*Received 16 December 2010; in final form 4 April 2011*)

A cationic porphyrin–anthraquinone hybrid and its Zn(II), Cu(II), Co(III), and Mn(III) complexes were synthesized and their interactions with duplex DNA were studied using a combination of absorption, fluorescence titration, circular dichroism spectroscopy, thermal DNA denaturation, viscosity measurements, gel electrophoresis, and gas chromatography. Metal coordination induces intermolecular steric hindrance and thus the metal hybrids have smaller DNA binding affinities than the free base hybrid; the steric hindrance could relax the intermolecular aggregation and increase $^1O_2$ generation of the metal hybrids. The DNA photocleavage abilities of these hybrids were investigated.

Keywords: Porphyrin–anthraquinone hybrid; DNA-binding; Steric hindrance; DNA photocleavage

1. Introduction

The design of small complexes that bind and react with DNA becomes important as we begin to delineate the expression of genetic information at a molecular level. An understanding of how to target DNA sites with specificity will lead to novel chemotherapeutics and also to a greatly expanded ability to probe DNA and develop highly sensitive diagnostic agents [1–5]. Transition metal complexes are at the forefront of these efforts. Stable, inert, and water-soluble complexes containing spectroscopically active metal centers are valuable in research of biological systems. Such metal complexes have been applied to probe both the structural and functional aspects of nucleic acid chemistry [6–8].

Porphyrin (Por) and anthraquinone (AQ) have become important molecules for nucleic acid research. A number of metalloporphyrins have been used in various fields of DNA study, such as DNA breaks [9, 10], probes of DNA structure [11], enhancement of restriction enzyme activity [12], and photoactive insecticides [13]. Research on AQ is increasing with the development of anthracycline antitumor antibiotics [14–16].

*Corresponding author. Email: zhaoping666@163.com

ISSN 0095-8972 print/ISSN 1029-0389 online
DOI: 10.1080/00958972.2011.585641

Biochemical evidence suggests that, in common with the anthracyclines, DNA is among the principal cell targets of these drugs and the pharmacological activities of some of these drugs (such as adriamycin and daunomycin) occur when a quinone-containing chromophore intercalates into the base pairs of the duplex DNA [17–19].

Covalently linked Por–quinone hybrids have been frequently reported to have rich photophysical character and are ideal biomimetic models for photosynthesis [20]. Our laboratory recently linked Por and AQ moieties with different lengths of flexible alkyl chains and found that these Por–AQ (Por–AQ) hybrids could bind and photocleavage duplex DNA efficiently [21]. Moreover, hybrids with long linkages could bis-intercalate into DNA base pairs with both Por and AQ moieties and especially have high DNA-binding affinities. Thus, these hybrids may have potential in designing new, highly efficient, anthracycline antitumor antibiotics.

As our continuing research, we synthesized the zinc(II) (**2**), copper(II) (**3**), cobalt(III) (**4**), manganese(III) (**5**) complexes of a cationic Por–AQ hybrid linked by an octanoyl group (**1**) (see molecular structures in figure 1) and investigated their binding behaviors with calf thymus DNA (CT DNA) and photocleavage properties with pBR322 plasmid DNA.

2. Experimental

2.1. *Materials and chemicals*

The free base Por–AQ hybrid **1** was prepared according to the literature method [21]. The metal complexes **2**, **3**, **4**, and **5** were prepared by mixing **1** with corresponding acetate salts in the dark [22]. The formation of the metal complexes was confirmed by TLC and UV-Vis absorption spectra.

The spectroscopic results obtained from **2**: ES-MS [EtOH, m/z]: 544 ($[M]^{2+}$), 363 ($[M]^{3+}$). (Found (%): C, 50.84; H, 4.17; N, 7.16. Calcd for $ZnC_{66}H_{55}I_3O_4N_8 \cdot 5H_2O$ (%): C, 50.80; H, 4.20; N, 7.18). ^{1}H NMR (300 MHz, DMSO): chemical shift δ: 11.88 (s, 1 H, NH–C=O), 9.51 (d, $J = 5.9$ Hz, 6 H, 2, 6-pyridinium), 9.38 (s, 4 H, β-pyrrole),

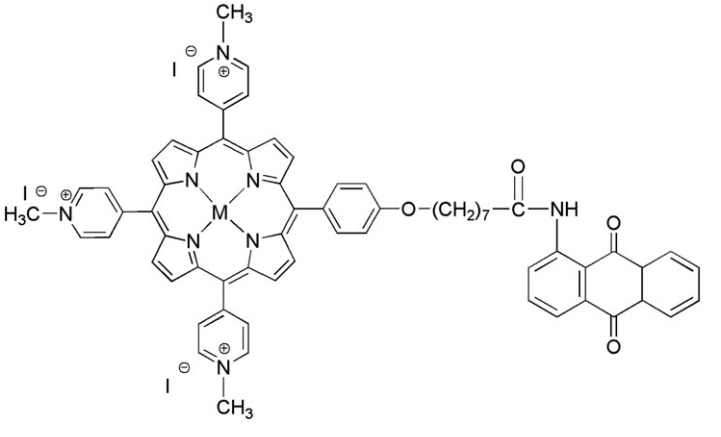

Figure 1. The molecular structures of **1–5**.

9.07 (s, 4 H, β-pyrrole), 8.92 (d, $J = 9.4$ Hz, 6 H, 3,5-pyridinium), 8.86 (s, 2 H, 2, 6-phenyl), 7.83 (s, 2 H, 3,5-phenyl), 7.65 (t, 4 H, AQ-phenyl), 7.33 (d, $J = 8.2$ Hz, 2 H, AQ-phenyl), 5.05 (s,1 H, AQ-phenyl), 4.67 (s, 9 H, N^+-Me), 4.25 (s, 2 H, $-CH_2-O$), 2.22 (s, 2 H, $-CH_2-C{=}O$), 1.18–1.89 (m, 10 H, $-(CH_2)_5-$). λ_{max} (nm) (log ε): 266 (4.9), 428 (3.72), 565 (3.48), 612 (3.04).

The spectroscopic results obtained from **3**: ES-MS [EtOH, m/z]: 542 ($[M]^{2+}$), 362 ($[M]^{3+}$). (Found (%): C, 52.09; H, 4.05; N, 7.38. Calcd for $CuC_{66}H_{55}I_3O_4N_8 \cdot 3H_2O$ (%): C, 52.07; H, 4.04; N, 7.36). λ_{max} (nm) (log ε): 267 (4.85), 429 (3.68), 547 (3.51), 594 (3.01).

The spectroscopic results obtained from **4**: ES-MS [EtOH, m/z]: 541 ($[M]^{2+}$), 361 ($[M]^{3+}$). (Found (%): C, 52.15; H, 3.74; N, 7.61. Calcd for $CoC_{66}H_{55}I_3ClO_4N_8 \cdot 3H_2O$ (%): C, 52.10; H, 3.78; N, 7.64). λ_{max} (nm) (log ε): 267 (4.85), 431 (3.72), 527 (2.96).

The spectroscopic results obtained from **5**: ES-MS [EtOH, m/z]: 538 ($[M]^{2+}$), 359 ($[M]^{3+}$). (Found (%): C, 52.18; H, 3.75; N, 7.68. Calcd for $MnC_{66}H_{55}I_3ClO_4N_8 \cdot 3H_2O$ (%): C, 52.24; H, 3.79; N, 7.66%). λ_{max} (nm) (log ε): 269 (4.87), 430 (3.72), 561 (3.48), 595 (3.02).

Buffer A (5 mmol L^{-1} Tris-HCl, 50 mmol L^{-1} NaCl, pH = 7.2, Tris = Tris (hydroxymethyl)aminomethane) solution was used in all the experiments except for thermal denaturation studies in which buffer B (1.5 mmol L^{-1} Na_2HPO_4, 0.5 mmol L^{-1} NaH_2PO_4, 0.25 mmol L^{-1} Na_2H_2EDTA ($H_4EDTA = N,N'$-ethane-1,2-diylbis [N-(carboxymethyl)glycine]), pH = 7.0) was used. Gel electrophoresis studies were carried out in buffer C (50 mmol L^{-1} Tris-HCl, 18 mmol L^{-1} NaCl, pH 7.2). CT DNA and pBR322 supercoiled plasmid DNA were obtained from the Sigma Company. A solution of CT DNA in buffer A gave a ratio of UV absorbance at 260 and 280 nm of 1.85 : 1, indicating that the DNA was sufficiently free of protein. The DNA concentration per nucleotide was determined by absorption spectroscopy using the molar absorption coefficient (6600 (mol $L^{-1})^{-1}$ cm^{-1}) at 260 nm [23]. Unless otherwise stated, reagents were commercially available and of analytical grade.

2.2. *Measurements*

UV-Vis spectra were recorded on a Perkin-Elmer-Lambda-850 spectrophotometer. Fluorescence spectra were recorded on a Perkin-Elmer L55 spectrofluorophotometer at room temperature. CD spectra were recorded on a JASCO-J810 spectrometer. Thermal denaturation studies were carried out with a Perkin-Elmer-Lambda-850 spectrophotometer equipped with a Peltier temperature-controlling programmer (±0.1°C). Melting curves were obtained by measuring the absorbance at 260 nm for solutions of CT DNA (100 μmol L^{-1}) in the absence and presence of the hybrids (10 μmol L^{-1}) as a function of temperature. The temperature was scanned from 40°C to 90°C at a speed of 1°C min^{-1}. The melting temperature (T_m) was taken as the mid-point of the hyperchromic transition.

For the gel electrophoresis experiment, a pencil-type high-pressure mercury lamp-light filter assembly was used. Yellow-light filter was used for visible light ($\lambda > 470$ nm) and purple filter for UV light ($\lambda < 350$ nm) [24]. The samples were analyzed by electrophoresis for 2.5 h at 80 V in Tris-acetate buffer containing 1% agarose gel. The gel was stained with 1 μg mL^{-1} ethidium bromide (EB) and photographed under

UV light. The integrated density values (IDV) were given by FluorChem 5500 software. The percentage of cleavage (C) was calculated according to equation (1)

$$C = \frac{D_{II} + 2D_{III}}{D_I + D_{II} + 2D_{III}}, \quad (1)$$

where D_I, D_{II}, and D_{III} are the IDVs of form I (supercoil form), form II (nicked form), and form III (linear form), respectively.

For the measurement of photosensitized production of singlet oxygen, the amount of singlet oxygen generated by photosensitization of the hybrid was determined by the measurement of the rate of reaction between singlet oxygen and 1,3-diphenylisobenzofuran (DPBF). The buffered solution containing a hybrid ($1\,\mu mol\,L^{-1}$) and DPBF ($100\,\mu mol\,L^{-1}$), prepared in the dark, was illuminated at the λ_{max}^{Soret} and 25°C, and a loss of absorbance at 415 nm was followed spectrophotometrically. No DPBF bleaching in the absence of the hybrids and no hybrid decomposition on illumination were observed.

Yields of singlet oxygen were estimated by reaction between singlet oxygen and 1,5-dimethylfuran (DMFU). The reaction was carried out in methanol solution which contains a hybrid ($100\,\mu mol\,L^{-1}$), DMFU ($0.1\,mol\,L^{-1}$), and pyridine ($0.6\,mol\,L^{-1}$). The reaction solution was illuminated by the mercury lamp with a yellow light filter to get visible light ($\lambda > 470$ nm). The concentration of DMFU was monitored by Gas Chromatography (GC-7890II) using nonane as an internal standard.

3. Results and discussion

3.1. *DNA-binding studies*

3.1.1. Absorption titrations. Association of the metal hybrids with CT DNA was examined by absorption titration in the UV-Vis range. DNA titration absorption spectroscopy of hybrid **2** is exampled in figure 2 to show the spectral change of these hybrids and analogous spectra were obtained in the case of **3**, **4**, and **5**. All physical data about the change of hybrids' absorption spectra in the presence of increasing amounts of CT DNA are given in table 1.

From figure 2 and table 1, one finds that with increasing DNA concentration, absorption spectra of the compounds in the Pors' Soret band are remarkably disturbed, with a hypochromism from 32.7% to 50.2% and a bathochromism from 5–12 nm. The magnitude of absorption spectral perturbation is an intuitional evidence for the DNA binding of Pors. The intercalation of Por into DNA base pairs is characterized by a red shift (>10 nm) and intensity decrease (up to 40%) in the Soret band of UV-Vis spectra; groove binding mode shows no (or minor) change in UV-Vis spectra while outside binding mode also exhibits red shift and intensity decrease in the Soret band of Pors [25, 26]. The large bathochromism and hypochromism of **3** (11 nm and 50.2%) indicate that its Por plane may intercalate into DNA, similar to the DNA-binding behavior of the free base **1**. However, the moderate or minor changes in the Soret band of **2**, **4**, and **5** suggest that the Por planes of these three hybrids may employ non-intercalative binding modes.

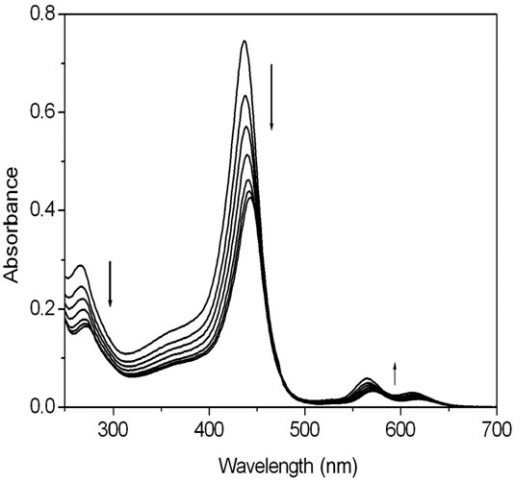

Figure 2. Absorption spectra of **2** in buffer A at 25°C in the presence of increasing amounts of CT DNA. [Hy] = 10 μmol L^{-1} ([Hy] refers to the concentration of the hybrid). [DNA] = 0, 2, 4, 6, 8, 10, 12 μmol L^{-1}. Arrows indicate the change in absorbance upon increasing DNA concentration.

Table 1. Physical data of Por–AQ hybrids binding with CT DNA.

	UV titration						
	Por moiety		AQ moiety				
Hybrid	Δλ (nm)	H%[a]	Δλ (nm)	H%	CD signal	ΔT_m (°C)	K_b
1	12	49.3	13	35.6	−	10.1	7.4×10^6
2	7	36.7	9	33.2	+	3.9	4.3×10^6
3	11	50.2	10	40.3	−	8.7	6.8×10^6
4	6	39.3	12	35.6	+ −	4.7	5.0×10^6
5	5	32.7	11	35.8	+ −	5.1	5.7×10^6

[a]H% refers to the hypochromism percentage.

The spectral changes of the AQ's characteristic absorption bands (ranging from 250 to 300 nm) were also monitored and the physical titration data for the AQ moiety are given in table 1. Upon addition of DNA, for all the metal hybrids, absorption spectra in this range have similar extent of change (large bathochromism and substantial hypochromism) with that of the free base hybrid **1**, which is a good DNA bis-intercalator. The large spectral perturbation indicates that the AQ planes in all these hybrids bind to DNA in a classic intercalative mode. It seems that the different metals in the Por core have no obvious effect on the DNA-binding behaviors of the AQ moiety. This result is consistent with the conclusion we made that the long bridging chain lengths of the Por–AQ hybrids decrease the steric hindrance between Por and AQ planes in the hybrid molecules and both the two moieties could bind with DNA freely [21].

3.1.2. Fluorescence titration. In a previous study, the fluorescence emission intensity of the free base hybrid **1** increased remarkably at both the Por's and AQ's characteristic

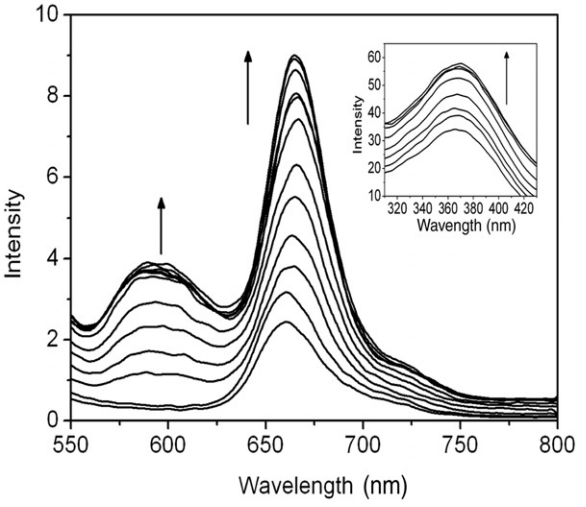

Figure 3. Emission spectra for Por moiety of **2** upon increasing CT DNA in buffer A. Inset: the emission spectra for AQ moiety of **2**. [Hy] = 10 μmol L^{-1}. [DNA] = 0–22 μmol L^{-1} from bottom to top. Arrows show the intensity change upon increasing DNA concentrations. $\lambda_{ex} = 449$ nm for the Por moiety and $\lambda_{ex} = 280$ nm for AQ moiety.

emission bands in the presence of CT DNA [21], which could be ascribed to DNA protection of the molecules from being quenched by water [27, 28]. Fluorescence titration experiments for the metal Por–AQ hybrids in the presence of CT DNA were performed. Large increases in fluorescence emission intensities are seen for **2** in the presence of increasing DNA (figure 3), which implies that Zn(II) hybrids can be protected by the hydrophobic environment inside the DNA helix.

Cu(II), Co(III), and Mn(III) hybrids **3**, **4**, and **5** show negligible luminescence in buffer A when excited at Por's or AQ's characteristic bands and negligible changes were found with the addition of DNA. The behaviors are closely related to the paramagnetism of these metal ions since they destroy the conjugated structure of the molecules [29–32]. For complexes exhibiting weak or no emission intensity in the presence of DNA, competitive binding to DNA with EB provides information regarding the nature of DNA binding [33, 34]. EB emits intense fluorescence in the presence of DNA, due to its strong intercalation between adjacent DNA base pairs [35]. The emission fluorescence of EB can be quenched by replacing the intercalated EB with other intercalating compounds, or it can occur indirectly by changing the DNA conformation as a result of binding with non-intercalating compounds. The quenching extent of direct EB replacement is always larger than the indirect DNA change [33–35].

With the increasing concentrations of the metal hybrids, the emission spectra of DNA-bound EB solution significantly quenched (figure 4). From figure 4, we find that **3** quenches the emission of EB to a greater extent than **4** and **5**. The much larger EB quenching of **3** suggests that the former may involve more intercalation in binding with DNA. Since the absorption titration results proved AQ of all these hybrids intercalate into DNA duplex, it is suggested that the Cu(II) hybrid **3** bis-intercalates into DNA duplexes while the Co(III) and Mn(III) hybrids **4** and **5** may only intercalate DNA with AQ.

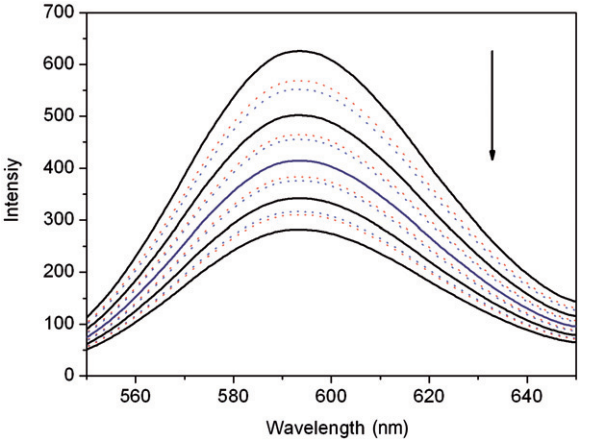

Figure 4. Fluorescence quench of DNA-bound EB with increasing concentration of **3** (—), **4** (- - -) and **5** (- - -) in buffer A. [DNA] = 50 μmol L^{-1}, [EB] = 8 μmol L^{-1}, λ_{ex} = 340 nm. [Hy] = 0, 2, 4, 6, 8 μmol L^{-1}. Arrows show the intensity change upon increasing concentrations of hybrids.

3.1.3. CD studies. CD spectra in the Soret region of Pors are well-defined and the least ambiguous indicators for the binding modes of Por compounds toward DNA. A positive CD peak is due to groove binding and a negative CD peak is due to intercalative binding, whereas a CD signal with both positive and negative peaks is ascribed to outside binding of Pors to DNA [25, 36].

Figure 5 illustrates the CD spectra and table 1 lists physical signals of the metal hybrids bound to CT DNA. None of these compounds by themselves as well as DNA displays any CD spectra signal in the visible region, but CD spectra are observed in the Soret band of these compounds with DNA titration.

The CD signal of **2** is dominantly positive and becomes stronger at higher DNA concentration, suggesting that the DNA binding of its Por moiety is primarily groove binding. The ellipticities of CD spectrum observed for Cu(II) hybrid **3** in the presence of DNA are predominantly negative in character and the negative signal becomes stronger with the addition of DNA. Since the negative CD signal is diagnostic of intercalative binding, this confirms that the Por of **3** intercalates into the DNA duplex under the experimental conditions. The substantial CD peaks with both positive and negative signals for **4** and **5** suggest that their Pors bind to DNA in an outside binding mode. The result of CD experiment proves the binding modes we proposed in the absorption and fluorescence experiments.

We have previously shown that the free base Por–AQ hybrid **1** bis-intercalates into DNA with its Por and AQ moieties [21]. From the foregoing CD results, we find that Cu(II) complexes of Por–AQ hybrid intercalate into DNA bases with its Por plane, while the Por moieties of Zn(II), Co(III), and Mn(III) only employ groove or outside binding modes when interacting with DNA. This may result from the four-coordinate structure of Cu(II) with no extra ligands on the axial position of the Por plane; Zn(II) has five-coordination with a water molecule as the axial ligand; Co(III), Mn(III) have six-coordination with a water molecule and a Cl^- as axial ligands [25, 37, 38]. The axial ligands of these hybrids increase the steric hindrance of the Por plane and thus, only the Por plane of the Cu(II) derivative, hybrid **3**, is sterically appropriate to bind with DNA in intercalative mode while the metal hybrids **2**, **4**, and **5** are not.

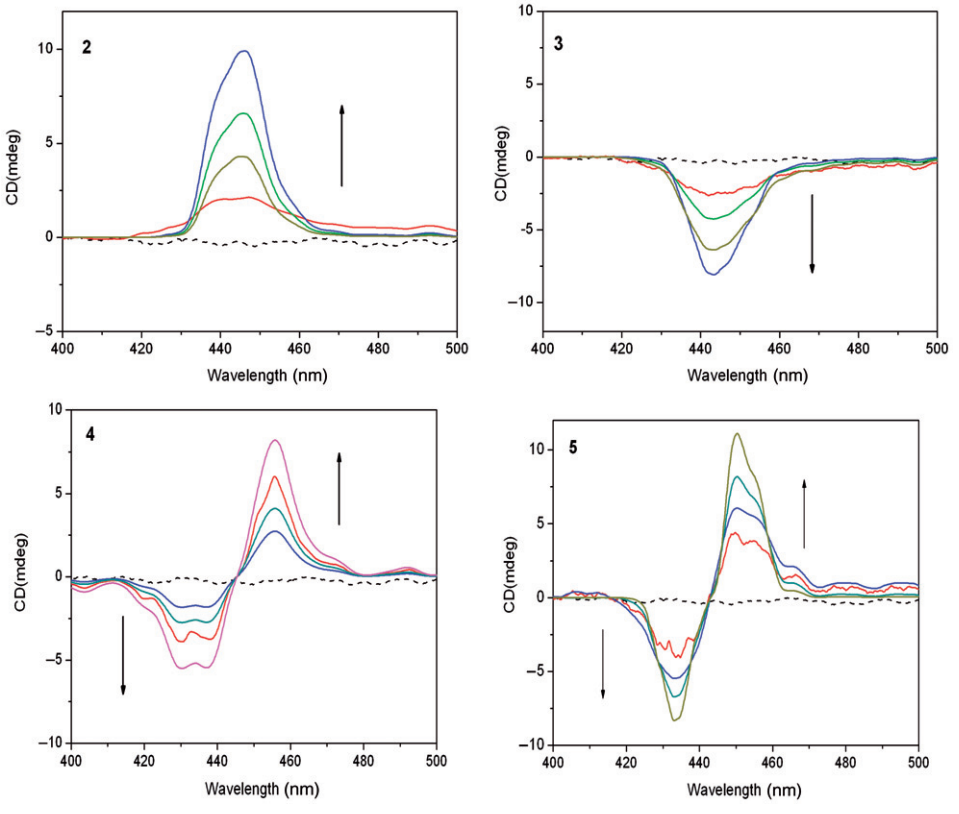

Figure 5. CD spectra at Por's Soret band in the absence (dashed lines) and presence (solid lines) of CT DNA in buffer A. [Hy] = 10 μmol L^{-1}. [Hy]/[DNA] = 0.3, 0.2, 0.15, 0.10, 0.05. Arrows indicate the change in CD spectra upon increasing DNA concentration.

3.1.4. Thermal denaturation studies. The melting temperature (T_m) of DNA is sensitive to its double helix stability and the binding of compounds to DNA alters the T_m depending on the strength of interactions. Therefore, it can be used as an indicator of binding properties of Pors to DNA and their binding strength. T_m will considerably increase when intercalation occurs [39].

The melting curves of CT DNA in the absence and presence of hybrids are presented in figure 6. The T_m of CT DNA is (61.1 ± 0.2)°C in the absence of the hybrids. When mixed with the hybrids at a concentration ratio [Hy]/[DNA] of 1 : 10 ([Hy] refers to the concentration of the hybrids), the observed melting temperatures of CT DNA increase to different extents. The differences, ΔT_m, are given in table 1. Here, $\Delta T_m = T_m - T_m^o$, T_m, and T_m^o refer to the melting temperature of DNA in the presence and absence of hybrids, respectively.

The large increases of T_m in the presence of **1** and **3** ($\Delta T_m = 10.1$°C and 8.7°C, respectively) indicate that intercalation occurs in the DNA binding of these two hybrids. Por and AQ planes of **1** intercalate into the DNA duplex and the similar large ΔT_m of **3** suggests that it also bis-intercalates with DNA. The increases of T_m in the presence of **2**, **4**, and **5** ($\Delta T_m = 3.9$°C, 4.7°C, and 5.1°C, relatively) are smaller than

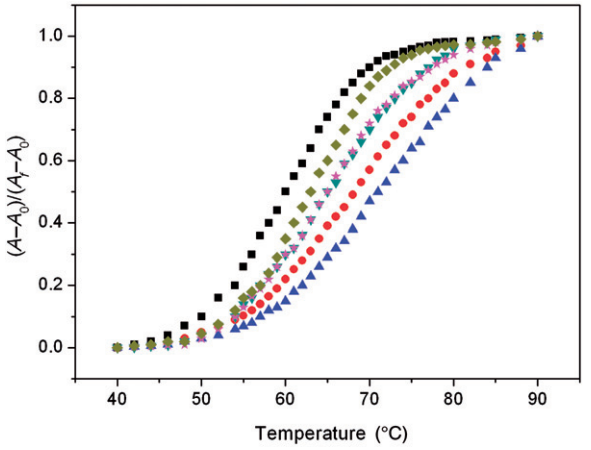

Figure 6. Melting curves of CT DNA at 260 nm in the absence (■) and presence of **1** (▲), **2** (♦), **3** (●), **4** (*), and **5** (▼) in buffer B. [Hy] = 10 μmol L^{-1}, [DNA] = 100 μmol L^{-1}.

those of **1** and **3**, indicating that DNA intercalation occurs in these hybrids but through only one plane. According to the results of CD experiment, the Por planes of **2**, **4**, and **5** do not intercalate into DNA. Thus, it could be concluded that the AQ planes of these metal hybrids intercalate into DNA duplex. These results are in good agreement with the absorption, fluorescence titration experiments given above.

3.1.5. Viscosity measurement. In the absence of X-ray structural data, viscosity measurement is regarded as a critical test of DNA binding in solution and provides strong arguments for intercalative DNA binding. Intercalation lengthens the DNA helix as the base pairs are pushed apart to accommodate the bound ligand, leading to an increase in DNA viscosity. In contrast, partial, non-classical intercalation of ligand could bend (or kink) the DNA helix and reduce its effective length and, concomitantly, its viscosity. When outside binding occurs, the viscosity of DNA will not change [40].

Figure 7 shows the effects of **1–5** on the viscosity of rod-like DNA, which is very sensitive to the binding modes of the ligands. On increasing the amounts of **1** and **3**, the relative viscosity of DNA increases steadily and significantly. The increases of **2**, **4**, and **5** also affect the relative viscosity of DNA. Similar to the results of DNA thermal denaturation, the DNA viscosity increase for **2**, **4**, and **5** are smaller than that of **1** and **3**, consistent with **1** and its Cu(II) derivative bis-intercalating between base-pairs of DNA, while the Zn(II), Co(III), and Mn(III) complexes only intercalate to DNA with the AQ. The results of viscosity experiments are consistent with the conclusion above.

3.1.6. The measurement of DNA binding constants. To quantitatively compare the DNA binding affinities of these hybrids, their binding constants (K_b) to CT DNA were measured. UV-Vis titration has several limitations in dealing with such compounds and fluorescence spectra were thus used to measure K_b of these hybrids by competition with EB to bind with DNA [21, 41, 42].

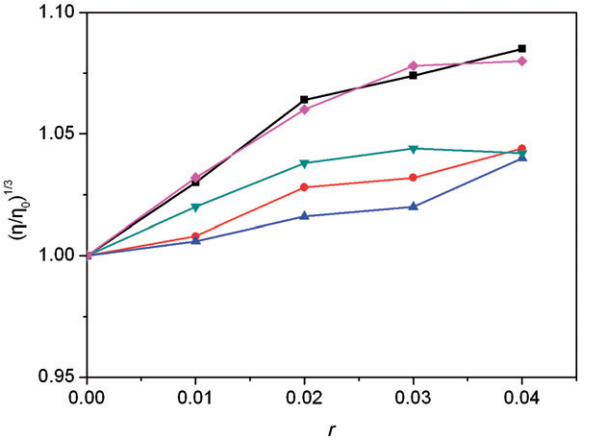

Figure 7. Plots of the relative viscosity change of CT DNA in the presence of **1** (■), **2** (●), **3** (♦), **4** (▲), and **5** (▼) in buffer A at (30 ± 0.1)°C. [DNA] = 0.5 mmol L^{-1}. η is the viscosity of DNA in the presence of the compounds and η_0 is the viscosity of DNA alone. r = [Hy]/[DNA].

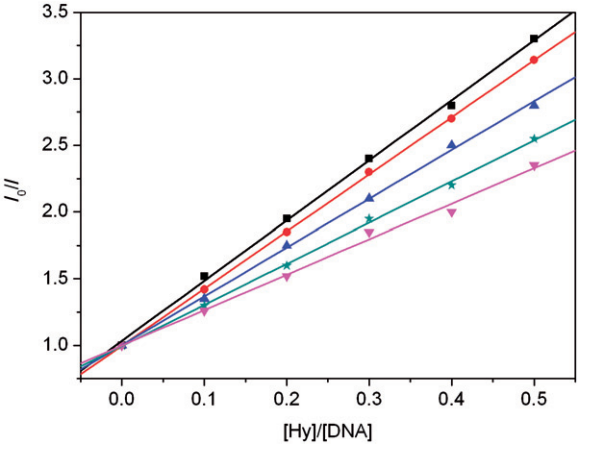

Figure 8. Fluorescence quenching plots of DNA-bound EB by Por–AQ hybrids, **1** (■), **2** (▼), **3** (●), **4** (*), and **5** (▲) in buffer A. [DNA] = 100 μmol L^{-1}, [EB] = 16.0 μmol L^{-1}, λ_{ex} = 537 nm.

EB competitive binding experiments were carried out and quenching plots are given in figure 8. The quenching plots of I_0/I *versus* [Hy]/[DNA] are in good agreement with the linear Stern–Volmer equation with slopes of 4.51, 2.65, 4.28, 3.08, 3.65 for hybrids **1–5**, respectively. From figure 8 50% of EB molecules were replaced from DNA bound EB at a concentration ratio [Hy]/[EB] = 1.35, 2.32, 1.47, 2.0, and 1.75 for hybrids **1–5**, respectively. By taking K_b of 1.0×10^7 mol L^{-1} for EB under this experimental condition [43], the K_b of the studied compounds were obtained (table 1) [44].

K_b of **1** and **3** are much larger than those of **2**, **4**, and **5**, because that both moieties in the long-linked hybrids intercalate into DNA and both can replace EB from the DNA helix, leading to relatively high binding affinities.

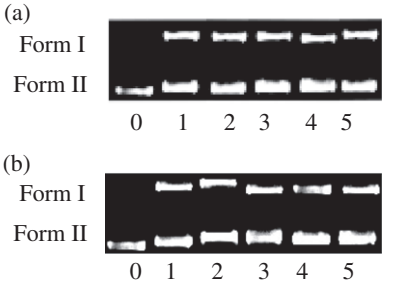

Figure 9. Photocleavage of pBR322 plasmid DNA after irradiation by (a) visible light ($\lambda > 470$ nm) in air or (b) UV light ($\lambda < 350$ nm) under an Ar atmosphere. Ten-microliter reaction mixtures containing 1.0 μg of plasmid DNA in buffer C. [Por] = 2 μmol L^{-1}. Lane 0: DNA controlled; Lanes 1–5: in the presence of hybrids **1**, **2**, **3**, **4**, and **5**, respectively, irradiation for 20 min.

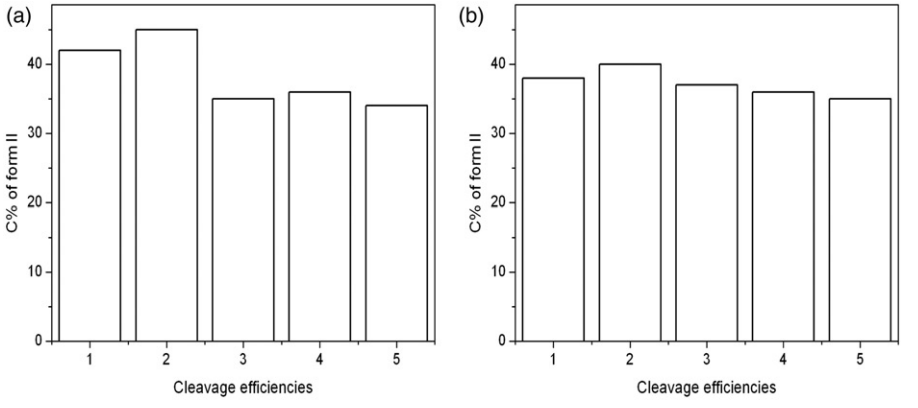

Figure 10. Photocleavage of pBR322 plasmid DNA after irradiation by (a) visible light in air or (b) UV light under an Ar atmosphere. Columns 1–5 for hybrids **1**, **2**, **3**, **4**, and **5**, respectively. The reaction conditions are the same as those in figure 9.

This research on DNA binding indicates that the metal coordinated with Por significantly influences the binding behavior of these Por–AQ hybrids to DNA.

3.2. *DNA photocleavage experiment*

Mehta *et al*. [45] reported that some non-charged Por–AQ hybrids are capable of displaying wavelength-dependent DNA cleavage and are valuable DNA photonucleases. To better understand the wavelength-dependent DNA photocleavage properties of these positively charged Por–AQ hybrids, we investigated the photocleavage of pBR322 plasmid DNA by **1–5** under irradiation with visible light (at Por's excitation wavelength) or UV light (at AQ's excitation wavelength), and the results are given in figure 9. The photocleavage percentages of **1–5** are shown in figure 10.

Without irradiation, no substantial DNA cleavage was observed for all the compounds (data not shown). Under irradiation with either visible or UV light, the

Table 2. Slopes of the plots of bleached absorption of DPBF and consumption of DMFU by photosensitization of hybrids.

	1	**2**	**3**	**4**	**5**
S_1[a]	0.24	0.35	0.29	0.34	0.33
S_1[b]	1.3	3.8	2.2	2.5	2.1

[a]S_1 refers to the slopes of the plots of bleached absorption of DPBF *vs.* illumination time. $[S_1] = \text{min}^{-1}$.
[b]S_2 refers to the consumption of DMFU *vs.* illumination time. $[S_2] = \times 10^{-4}\,\text{mol}\,\text{min}^{-1}$.

difference of DNA photocleavage efficiencies for these cationic hybrids was not so large, with **1** and **2** showing a little higher cleavage percentage than those of **3**, **4**, and **5**. DNA photocleavage activities of small molecules are closely related to their DNA binding modes and binding affinities. Intercalative mode and high DNA binding affinity are more advantageous in DNA cleaving [46–48]. The photocleavage efficiency obtained from figures 9 and 10 somewhat conflict with the above conclusion since **1** and **3** have higher DNA binding affinities and intercalative DNA binding. This could be explained by the following research.

Our previous study proved that $^1O_2$ was responsible for DNA photocleavage by the Por moiety of this kind of hybrid [21]. Photosensitized production of $^1O_2$ was estimated quantitatively by measuring the decomposition of DPBF and the concentration consumption of DMFU [49, 50]. The slopes of the plots of bleached absorption of DPBF and the consumption of DMFU *versus* illumination time are listed in table 2. Specific changes are given in "Supplementary material" (figures S1 and S2). From table 2 Zn(II) complexes show higher $^1O_2$ yields than Cu(II), Co(III), and Mn(III) complexes, consistent with previous reports and closely related to the lifetimes of the first excited triplet state of these metal complexes [51]. Moreover, the $^1O_2$ yields of the metal complexes are larger than that of the free base hybrid, indicating that the insertion of metal ions into the cationic Por enhanced $^1O_2$ production. It is widely accepted that long-linked cationic Por–drug hybrids easily form intermolecular dimer through self-aggregation in aqueous buffer. The dimers are inactive in yielding $^1O_2$ since the generated $^1O_2$ could be easily quenched by the aggregated molecules [52, 53]. Metal ions in the Por cores could induce severe steric hindrance between molecules which will efficiently relax the intermolecular self-aggregation and thus increase $^1O_2$ generation. Here, the steric hindrance derived from the insertion of metals into Por acts as a "double-edged sword" in the DNA photocleavage reaction, bringing less advantageous DNA binding but higher $^1O_2$ productivity for the hybrids than the metal-free one.

4. Conclusions

Based on absorption, fluorescence, circular dichroism spectroscopy, thermal denaturation, and viscosity measurements, the binding modes of Zn(II), Cu(II), Co(III), Mn(III) Por–AQ to CT DNA were compared with the free hybrid, which could bis-intercalate DNA duplex with both Por and AQ moieties. Among the four metal complexes, only Cu(II) hybrid could bis-intercalate into DNA, while the other three

Figure 11. The binding modes of cationic Por–AQ hybrids to CT DNA: (a) for **1** and **3**; (b) for **2**; (c) for **4** and **5**.

complexes, Zn(II), Co(III), and Mn(III) hybrids, bind to DNA with both intercalative mode (AQ plane) and groove or outside mode (Por plane) (figure 11). This can be understood by Cu(II) having no axial ligands when coordinating with the Por plane while Zn(II), Co(III), Mn(III) have H_2O or Cl^- in axial positions. The metal complexes have higher singlet oxygen ($^1O_2$) production than **1**, because insertion of metals into Por planes could induce steric hindrance between molecules, efficiently relaxing the intermolecular aggregation. These results are helpful in understanding DNA interactions of small molecules and may facilitate the design of new anticancer drugs.

Acknowledgments

This work was financially supported by Guangdong Pharmaceutical University and the Medical Research Foundation of Guangdong (B2010158).

References

[1] M. Kalek, A.S. Madsen, J. Wengel. *J. Am. Chem. Soc.*, **129**, 9392 (2007).
[2] A. Bagno, G. Saielli. *J. Am. Chem. Soc.*, **129**, 11360 (2007).
[3] E.A. Lukyanets, V.N. Nemykin. *J. Porphyrins Phthalocyanines*, **14**, 1 (2010).
[4] E. Almaraz, Q.A. de Paula, Q. Liu, J.H. Reibenspies, M.Y. Darensbourg, N.P. Farrell. *J. Am. Chem. Soc.*, **130**, 6272 (2008).
[5] G.A. Cisneros, L. Perera, R.M. Schaaper, L.C. Pedersen, R.E. London, L.G. Pedersen, T.A. Darden. *J. Am. Chem. Soc.*, **131**, 1550 (2009).
[6] L.N. Ji, X.H. Zou, J.G. Liu. *Coord. Chem. Rev.*, **216–217**, 513 (2001).
[7] F.R. Keene, J.A. Smith, J.G. Collins. *Coord. Chem. Rev.*, **253**, 2021 (2009).
[8] A.M. Pizarro, P.J. Sadler. *Biochimie*, **91**, 1198 (2009).
[9] E. Fouquet, J. Bernadou, B.J. Meunier, G. Pratviel. *Chem. Commun.*, **15**, 1169 (1987).
[10] D.K. Deda, A.F. Uchoa, E. Caritá, M.S. Baptista, H.E. Toma, K. Araki. *Int. J. Pharm.*, **376**, 76 (2009).
[11] B. Ward, A. Skorobogarty, J.C. Dabrowiak. *Biochemistry*, **25**, 6875 (1986).
[12] M. Tabata, K. Nakajima, E. Nyarko. *J. Inorg. Biochem.*, **78**, 383 (2000).
[13] L. Guo, W.J. Dong, X.F. Tong, C. Dong, S.M. Shuang. *Talanta*, **70**, 630 (2006).
[14] R.E. McKnight, J.G. Zhang, D.W. Dixon. *Med. Chem. Lett.*, **14**, 401 (2004).
[15] G.S.B. Vernon. *J. Mol. Graphics Modell.*, **26**, 14 (2007).
[16] P. Wardman. *Clin. Oncol.*, **19**, 397 (2007).
[17] A. DiMarco, R. Silverstrini, M. Soldati, P. Orezzi, T. Dasdia, B.M. Scarpinato, L. Valentini. *Nature*, **201**, 706 (1964).
[18] Y.K. Liaw, V.M. Li, J.H. Boom, A.H. Wang. *Proc. Natl Acad. Sci. USA*, **88**, 4845 (1991).
[19] K. Atsushi, G. Tomoko, N. Shigeo, I. Toshihiro, T. Makoto. *Chem. Lett.*, **30**, 370 (2001).
[20] M.R. Wasielewski. *Chem. Rev.*, **92**, 435 (1992).
[21] P. Zhao, L.C. Xu, J.W. Huang, K.C. Zheng, B. Fu, H.C. Yu, L.N. Ji. *Bioorg. Chem.*, **36**, 278 (2008).
[22] C. Casas, B. Saint-Jalmes, C. Loup, C.J. Lacey, B. Meunier. *J. Org. Chem.*, **58**, 2913 (1993).

[23] M.E. Reichmann, S.A. Rice, C.A. Thomas, P. Doty. *J. Am. Chem. Soc.*, **76**, 3047 (1954).
[24] C.J. Sansonetti, M.L. Salit, J. Reader. *Appl. Opt.*, **35**, 74 (1996).
[25] R.F. Pasternack, E.J. Gibbs, J.J. Villafranca. *Biochemistry*, **22**, 2406 (1983).
[26] D.R. McMillin, A.H. Shelton, S.A. Bejune, P.E. Fanwick, R.K. Wall. *Coord. Chem. Rev.*, **249**, 1451 (2005).
[27] J.S. Trommel, L.G. Marzilli. *Inorg. Chem.*, **40**, 4374 (2001).
[28] L.N. Ji, X.H. Zou, J.G. Liu. *Coord. Chem. Rev.*, **216–217**, 513 (2001).
[29] R.S. Becker, M. Kasha. *J. Am. Chem. Soc.*, **77**, 3669 (1955).
[30] K.M. Smith. *Porphyrins and Metalloporphyrins*, p. 667, Elsevier, New York (1975).
[31] J.Z. Lu, J.W. Huang, L.F. Fan, J. Liu, X.L. Chen, L.N. Ji. *Inorg. Chem. Commun.*, **7**, 1030 (2004).
[32] T. Li, J.W. Huang, L. Ma, Y.Q. Zhang, L.N. Ji. *Transition Met. Chem.*, **28**, 288 (2003).
[33] B.C. Baguley, M. Lebret. *Biochemistry*, **23**, 937 (1984).
[34] J.R. Lakowicz, G. Webber. *Biochemistry*, **12**, 4161 (1973).
[35] J.B. Lepecp, C. Paoletti. *J. Mol. Biol.*, **27**, 87 (1967).
[36] R.F. Pasternack, P. Garrity, B. Ehrlich, C.B. Davis, E.J. Gibbs, G. Orloff, A. Giartosio, C. Turano. *Nucleic Acids Res.*, **14**, 5919 (1986).
[37] M. Tabata, A.K. Sarker, E. Nyarko. *J. Inorg. Biochem.*, **94**, 50 (2003).
[38] F.R. Keene, J.A. Smith, J.G. Collins. *Coord. Chem. Rev.*, **253**, 2021 (2009).
[39] H.T. Daryono, M. Shunsuke, A. Takehiro, Y. Naoki, I. Hidenari. *J. Inorg. Biochem.*, **85**, 219 (2001).
[40] S. Satyanarayana, J.C. Dabrowiak, J.B. Chaires. *Biochemistry*, **32**, 2573 (1993).
[41] M.A. Sari, J.P. Battioni, D. Dupre, D. Mansuy, J.B. Lepecq. *Biochemistry*, **29**, 4205 (1990).
[42] T. Jia, Z.X. Jiang, K. Wang, Z.Y. Li. *Biophys. Chem.*, **119**, 295 (2006).
[43] Y.Y. Fang, B.D. Ray, C.A. Caussen, K.B. Lipkowitz, E.C. Long. *J. Am. Chem. Soc.*, **126**, 5403 (2004).
[44] M.J. Han, L.H. Gao, Y.Y. Lu, K.Z. Wang. *J. Phys. Chem. B*, **110**, 2364 (2006).
[45] G. Mehta, S. Muthusamy, B.G. Maiya, S. Arounaguiri. *Tetrahedron Lett.*, **38**, 7125 (1997).
[46] T. Jia, Z.X. Jiang, K. Wang, Z.Y. Li. *Biophys. Chem.*, **119**, 295 (2006).
[47] H. Taima, A. Okubo, N. Yoshioka, H. Inoue. *Chem. Eur. J.*, **12**, 6331 (2006).
[48] B. Chen, W. Qin, P. Wang, T. Tian, H.J. Ma, X.P. Cao, X.J. Wu, X. Zhou, X.L. Zhang, F. Liu, F. Zheng, X. Li. *Bioorg. Med. Chem. Lett.*, **13**, 3731 (2003).
[49] S.K. Wu, H.C. Zhang, C.G. Zhu, D.N. Xu, H.J. Xu. *Acta Chim. Sin.*, **43**, 10 (1985).
[50] J.D. Huang, E.S. Liu, S.L. Yang, D.F. Wu, N.S. Chen, J.L. Huang. *J. Xiamen Univ.*, **36**, 399 (1997).
[51] J.R. Darwent, P. Douglas, A. Harriman, G. Porter, M.-C. Richoux. *Coord. Chem. Rev.*, **44**, 83 (1982).
[52] Y. Ishikawa, N. Yamakawa, T. Uno. *Bioorg. Med. Chem.*, **10**, 1953 (2002).
[53] N. Yamakawa, Y. Ishikawa, T. Uno. *Chem. Pharm. Bull.*, **49**, 1531 (2001).